



Colloidal titania-silica-iron oxide nanocomposites and the effect from silica thickness on the photocatalytic and bactericidal activities[☆]



Padtaraporn Chanhom^a, Nisanart Charoenlap^b, Boosayarat Tomapatanaget^a, Numpon Insin^{a,*}

^a Department of Chemistry, Faculty of Science, Chulalongkorn University, Bangkok 10330, Thailand

^b Laboratory of Biotechnology, Chulabhorn Research Institute, Bangkok 10210, Thailand

ARTICLE INFO

Keywords:

Photocatalyst
Nanocomposite
Superparamagnetic
Titania

ABSTRACT

New types of colloidal multifunctional nanocomposites that combine superparamagnetic character and high photocatalytic activity were synthesized and investigated. The superparamagnetic nanocomposites composed of anatase titania, silica, and iron oxide nanoparticles (TSI) were synthesized using thermal decomposition method followed by microemulsion method, without calcination at high temperature. Different techniques including X-ray diffraction (XRD) and transmission electron microscope (TEM) were used to characterize and confirm the structure of the nanocomposites. These nanocomposites showed high photocatalytic activity when used in the photodegradation of methylene blue under irradiation with a black light lamp. Moreover, the nanocomposites exhibited high antibacterial properties. From our study, the nanocomposites can be useful in various applications such as removal of pollutants with readily separation from the environment using an external magnetic field. These composites could effectively photo-degrade the dye at least three cycles without regeneration. The effects of silica shell thickness on the photocatalytic activity was investigated, and the thickness of 6 nm of the silica interlayer is enough for the inhibition of electron translocation between titania and iron oxide nanoparticles and maintaining the efficiency of photocatalytic activity of titania nanoparticles.

1. Introduction

Titania or titanium oxide (TiO₂) has become an attractive material for applications in different fields ranging from photocatalysis to medicine. The photocatalytic process has been reported to be more effective in the degradation of organic pollutants than other processes [1], and titania nanoparticles are one of the most interesting photocatalysts. The important advantages of titania are as follows [2,3]. First, titania is an excellent photocatalyst because it shows high photocatalytic activity in various reactions. Also, titania has physical and chemical stability; accordingly, it can destroy a variety of organic pollutants in different solutions without reduction in the catalytic activity and can be reused for many cycles. Moreover, titania is inexpensive, and non-toxic material that can transform a variety of toxic pollutants into harmless products. However, the post-treatment separation in titania slurry system after photocatalytic oxidation reaction has a serious limitation as it is difficult to separate and recover titania nanoparticles from the liquid phase. In order to solve this problem, one of the alternative approaches is coating titania particles on the surface of magnetic particles to equip them with magnetic responses for magnetic separation.

The two-component model, in which titania particles were directly coated onto the magnetic particles to form the magnetic particles/titania particles core/shell structures, has been reported [4]. Maghemite and magnetite particles were commonly used as the magnetic components due to their stability toward oxidation and low toxicity. However, low photocatalytic activity was observed because a direct contact of the magnetic core and titania shell could increase to the recombination of photogenerated electron-hole pairs [4,5]. The drawback could be overcome by inserting an interlayer comprising materials with large band gap to inhibit the recombination of electron-hole pairs for improving the photocatalytic activity. For this purpose, silica has been reported to be used as interlayer because other than its large band gap, silica exhibits high thermal and chemical stability and low toxicity [6].

The three-component structures of the magnetic core/insulator interlayer/photocatalyst shell composites composed of iron oxides/silica/titania have been reported to obtain a photocatalyst with high photocatalytic activity in combination with strong magnetic responses [6,7]. However, in these previous studies the three-component composites were in the size range of 300–550 nm or larger in diameters, at which the composites were likely to aggregate readily due to the

[☆] In remembrance of His Majesty King Bhumibol Adulyadej (1927–2016), for his life-time dedication to Thailand.

* Corresponding author.

E-mail address: Numpon.I@chula.ac.th (N. Insin).

magnetic dipole interaction of each particle and low colloidal stability for the particles of large sizes. In order to reduce the aggregation and increase the surface area and photocatalytic activity of the composites, the sizes of the composites should be smaller with the iron oxides components are in their superparamagnetic state where the magnetic attraction between particles is not observed. It has been reported that the magnetite and maghemite nanoparticles with the size ranging from 4 to 50 nm in diameter exhibit superparamagnetic character [8–13] and the magnetic photocatalyst should incorporate the iron oxides nanoparticles of these sizes to become colloidally stable.

In this work we have synthesized superparamagnetic iron oxide/silica/titania nanocomposites that were colloidally stable in order to diminish particle agglomeration using a combination of thermal decomposition and reverse microemulsion methods. Superparamagnetic iron oxide nanoparticles, prepared by thermal decomposition of iron-oleate complex, were encapsulated inside discrete silica nanospheres, and titania was coated onto surface of silica using the reverse microemulsion method. Under mild conditions, titania was transformed from amorphous phase to anatase, resulting in the titania-silica-iron oxide nanocomposites (TSI) with low aggregation, high colloidal stability and low energy consumption in the preparation. The photocatalytic properties of as-synthesized core-shell nanocomposites were evaluated by the degradation of methylene blue under UV irradiation. Also, titania has been reported to kill bacteria because of their photocatalytic activity [14]; therefore, the bactericidal activity of the new magnetic titania nanocomposites was investigated using a Gram-positive *Staphylococcus aureus* as a model. *S. aureus* is a human pathogenic bacterium, which is defined as one of the major causes of healthcare-associated Infections (HAI) by Center of Control Diseases (CDC) [15]. *S. aureus* causes many diseases, including bacteremia [16], pneumonia [17], and endocarditis [18], especially in immunocompromised or immunosuppressed patients who are hospitalized for a long period of time. Moreover, *S. aureus* has ability to acquire antibiotic resistances from other organisms, resulting in high number of resistant *S. aureus* strains that is more difficult to cure with antibiotic. This life-threatening infection is currently of a major concern worldwide. Thus, other than searching for new antibiotics, a novel strategy for treatment of *S. aureus* infection should be considered.

2. Experimental section

2.1. Materials

Iron (III) chloride hexahydrate ($\text{FeCl}_3 \cdot 6\text{H}_2\text{O}$), 1-octadecene, Igepal CO-520, Tetrabutyl orthotitanate (TBOT) were purchased from Aldrich. Tetraethyl orthosilicate (TEOS) and Cetyltrimethylammonium bromide ($\text{C}_{19}\text{H}_{42}\text{BrN}$, CTAB) were purchased from Fluka. All chemical reagents were of analytical grade and used without further purification.

2.1.1. Syntheses of nanocomposites

The synthesis of monodisperse iron oxide nanoparticles (I) was performed using a method reported earlier with some modification [8,9]. 8 mmol of iron (III) chloride was dissolved in de-ionized water (10 mL). 24 mmol of sodium oleate was transferred into the iron (III) chloride solution. Then, 56 mL mixture of ethanol, de-ionized water, and hexane (the volume ratio of ethanol:water:hexane=1.33:1:2.33) were added to the above solution, and the mixture was refluxed at 70 °C for 4 h. After being washed in de-ionized water for three times, the resulting iron-oleate complex was collected using centrifugation. Then, hexane was removed by evaporation under reduced pressure. The sticky iron-oleate complex precursor was dispersed in a mixed solvent comprising oleic acid and 1-octadecene with the weight ratio of oleic acid:iron-oleate complex:1-octadecene of 1:6.3:35. The mixture solution was slowly heated to 320 °C and maintained at that temperature for 30 min under nitrogen gas. Iron oxide nanoparticles were

precipitated and collected by centrifugation.

Tetraethyl orthosilicate (TEOS) was used as silicon source for the preparation of silica-coated iron oxide nanoparticle (SI) using the reverse microemulsion method similar to previous reports [19,20]. Typically, 9.88g of Igepal CO-520 was dispersed in cyclohexane by sonication. Then, 90 mg of iron oxide nanoparticles were added to solution under continuous stirring. Afterward, 700 μL of 25% ammonium hydroxide solution and 600 μL of TEOS were added to the above mixture solution. The reaction was continually stirred for 16 h at room temperature. Finally, the silica-coated iron oxide nanoparticles were precipitated in ethanol using centrifugation.

In the preparation of silica-coated iron oxide nanoparticles, the effect of the amount of TEOS on the thickness of silica shell was investigated. The process of silica thickness variation was done following the method above but varied amounts of TEOS were added in the mixture solution. Three different volumes of TEOS (150, 600 and 2400 μL) were used in preparation of silica layer. The SI nanocomposites of different silica thickness were further coated with titania.

The reverse microemulsion method for coating titania nanoparticle on the silica-iron oxide surface to obtain titania-silica-iron oxide nanocomposites (TSI) was modified from previous research [21]. Firstly, 7.3 mL of 1-hexanol was used as solvent for dispersing as-synthesized silica-coated iron oxide (SI) nanoparticles. 3g of cetyltrimethylammonium bromide (CTAB) was added to the silica-coated iron oxide solution. Secondly, the mixed solution was continuously stirred at room temperature for 1 h. Afterward, 50 μL of tetrabutyl orthotitanate (TBOT) and 1 mL of de-ionized water were added into the mixture. The reaction mixture was refluxed at 80 °C for 24 h under vigorous stirring. Finally, the sample was centrifuged and washed with ethanol and de-ionized water, and the final product was re-dispersed in PBS buffer (pH 7.4) for bactericidal activity. For comparison, titania-coated iron oxide nanoparticles (TI) and pure titania photocatalyst (T) were prepared in the same method mentioned above.

2.2. Characterization methods

2.2.1. X-ray Electron Diffraction (XRD)

The crystalline phases of iron oxides and titania nanoparticles were characterized using a D/MAX 2200 X-ray diffractometer (Rigaku, Japan) with Cu-K α radiation at an accelerating voltage of 40 kV and an applied current of 30 mA. The XRD patterns of composites, iron oxides and titania nanoparticles were recorded at 2θ in a range of 20–80°.

2.2.2. Transmission electron microscopy (TEM)

TEM images were taken using a JEOL 2100 microscope (Japan) at an accelerating voltage of 120 kV. One drop of the colloidal solutions, prepared by dispersing a small amount of nanoparticles in ethanol using an ultrasonic treatment for at least 2 min, was placed onto a formvar-coated copper grid and dried at room temperature for TEM measurement. The images were used to study the sizes and morphology of particles and the thickness of the coating of the layers.

2.3. Measurement of photocatalytic activity

The photocatalytic activity of the as-prepared nanocomposite was investigated by measuring the degradation of methylene blue solution upon UV irradiation and comparing with the titania-coated iron oxide nanoparticles and iron oxide nanoparticles. A 36 W black light blue UV lamp was used as the irradiation light source. For each photocatalytic experiment, photocatalyst nanocomposites with 45 mg of iron oxide nanoparticles were dispersed in a 30 mL aqueous solution of 12 ppm methylene blue. The suspension was kept in dark to obtain an adsorption-desorption equilibrium for the catalyst, water and dye before irradiation. At given intervals of UV irradiation for 0–5 h, sample was collected, and the catalyst was separated from the solution

using a magnet. The photocatalytic ability of the as-prepared TSI nanocomposites was compared with the titania-coated iron oxide nanoparticles and iron oxide nanoparticles by determining the photodegradation of methylene blue measured by the decrease of the dye absorbance at 664 nm.

The catalyst reusability was investigated by repeating the photocatalytic cycles of the same TSI catalyst. The reused catalyst experiment was done according to the measurement of photocatalytic activity mentioned earlier. The catalyst was collected from methylene blue solution using a magnet. The photocatalytic cycle was repeated for three times.

2.4. Bactericidal activity

In order to determine the bactericidal activity of TSI nanocomposite, the killing assay [22] was performed with some modifications. Briefly, *S. aureus* was grown aerobically in 5 mL of Luria-Bertani (LB) broth at 37 °C overnight with shaking. Then, the cells were subcultured in 20 mL of fresh LB medium and grown until reaching exponential phase (optical density at 600 nm of 0.5). The cells were then treated with nanocomposite activated by Ultra Violet (UV) light (200 lx, measured using a digital light meter, Model EA31, Exttech Instrument, USA) at 37 °C for 1 h. The treated cells were serially diluted in LB and 10 μ L of each sample was spotted on the LB agar plate. The plates were incubated at 37 °C for 24 h under UV light before the survival colonies were counted. The cells treated with UV radiation alone were used as a control experiment and conducted in parallel. All experiments were repeated at least three times and representative data are shown.

3. Results and discussion

The titania-silica-iron oxides nanocomposites were prepared from hydrothermal decomposition of iron oleate complexes and reverse microemulsion, resulting in brown powder after centrifuged and dried under reduced pressure. The crystalline phases of the nanocomposites were identified using X-ray diffractometry. Fig. 1 shows the XRD patterns of iron oxide nanoparticles, titania nanoparticles, titania-silica-iron oxide nanoparticles, and titania-coated iron oxide nanoparticles. The diffraction peaks for the magnetite (JCPDS no. 19-0629) and anatase phase (JCPDS no. 21-1272) are marked with circle and triangle signs, respectively. From the XRD pattern of iron oxide nanoparticles (Fig. 1a), it shows a set of strong XRD peaks at $2\theta=20\text{--}80^\circ$ corresponding to magnetite phase [8]. The XRD patterns of titania nanoparticles (Fig. 1b) show that the as-prepared titania nanoparticles have diffrac-

tion peaks at the same position as the characteristic diffraction peaks of anatase titania (2θ at 25.5°, 37.9°, 48.2° and 54.4°). Fig. 1c and d present XRD patterns of titania-silica-iron oxide nanoparticles and titania-coated iron oxide nanoparticles, respectively. The XRD patterns show that both composites have mixed diffraction peaks of anatase and magnetite phase, suggesting that the phase structure of iron oxide nanoparticles are well retained after coating the outer shell with silica and titania. It can be indicated that the composites could have both the ferrimagnetic property from iron oxide nanoparticles [8] and the high photoactive property from titania of anatase phase [2].

The TEM images for the samples that obtained at different experimental conditions are shown in Fig. 2. The TEM image of the iron oxide nanoparticles prepared by thermal decomposition procedure showed narrow size distributions and spherical shape as shown in Fig. 2a. These particles can disperse well in nonpolar solvents. The particle size of as-prepared iron oxide nanoparticles has diameters ranging from 8 to 12 nm. After deposition of silica layer onto iron oxide nanoparticles, most silica shells were uniformly coated on the surface of iron oxide nanoparticles as shown in Fig. 2b. The image displays a strong evidence of a core-shell structure that the iron oxide core (dark) is surrounded by a thin silica shell (bright). In contrast, the titania-coated iron oxide nanocomposites showed some degree of agglomeration and the titania shells were not clearly observed by TEM image (Fig. 2c). This is likely due to the fact that reaction rate of TBOT is much faster and more difficult to control compared to TEOS.

For the variation in the thickness of silica layer, the quantities of TEOS were adjusted resulting in different thicknesses of silica layers according to Table 1 and Fig. 2d–f. The mean thicknesses of silica layer from TEM images were approximately 1.1 ± 0.5 nm (Sample A), 6.1 ± 1.2 nm (Sample B) and 16.6 ± 2.0 nm (Sample C) directly depending on the quantity of TEOS added. After further titania coating, TEM images of titania-silica-iron oxide nanoparticles was recorded as shown in Fig. 2d–f. It can be seen that titania shells from the hydrolyzed tetrabutyl orthotitanate (titanium source) was deposited uniformly onto the surface of the silica-coated iron oxide nanoparticles. Fig. S2 (Supplementary) displays that confirmation of titania coating on the nanocomposites using elemental mapping (using $K\alpha$ signal of Ti) from Energy dispersive X-ray spectroscopy elemental analysis. All prepared nanocomposites prepared exhibited a mean diameter of less than 100 nm.

The magnetic properties of the products were investigated using a vibrating sample magnetometer (VSM; Model 7404, Lake Shore Cryotronics, Inc., USA) as a magnetization curves in Fig. S3 in Supplementary. All of the materials showed superparamagnetic behavior at room temperature as there was no coercivity observed. The saturation magnetization (M_s) of the iron oxide (I) nanoparticle was 58 emu/g corresponding to magnetite nanoparticles with excess oleic acid surfactant [20], whereas those of titania-coated iron oxide (TI) nanoparticle and titania-silica-iron oxide (TSI) nanoparticle were 8 and 7 emu/g, respectively. The significant decreases in M_s of TI and TSI in comparison to iron oxide nanoparticles are as expected for the composite materials between ferrimagnetic materials and diamagnetic materials.

Photodegradation of methylene blue under UV irradiation was studied in order to compare the photocatalytic activities of the photocatalysts. As shown in Fig. 3, comparing five catalysts, the TSI_Sample B and Sample C nanocomposites exhibited high photocatalytic efficiency of above 95% dye degradation in 5 h of irradiation. However, only 76.9% methylene blue was decomposed using TSI_Sample A as photocatalyst under the same condition, and only 6.29% and 3.13% methylene blue decomposition was observed when TI nanocomposite and iron oxide nanoparticles were used as photocatalysts, respectively. From the reported band edge positions of the three materials [23–25], an unfavorable electronic heterojunction between iron oxide core and titania shell was expected and could lead to higher possibility of electron-hole recombination. Iron oxide core becomes the

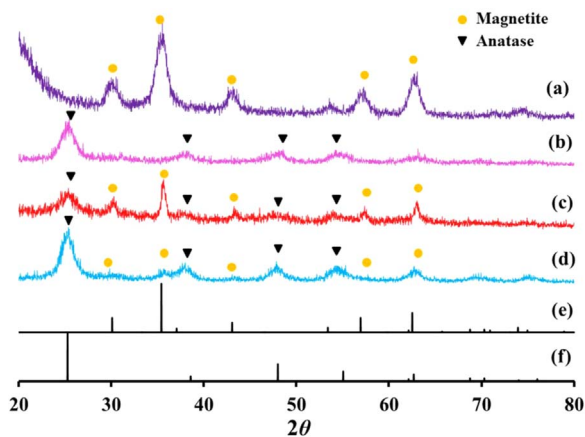


Fig. 1. X-ray diffraction patterns of (a) iron oxide nanoparticles, (b) titania nanoparticles, (c) titania-silica-iron oxide (TSI) nanoparticles, (d) titania-coated iron oxide (TI) nanoparticles, (e) JCPDS no. 19-0629 (magnetite phase), (f) JCPDS no. 21-1272 (anatase phase).

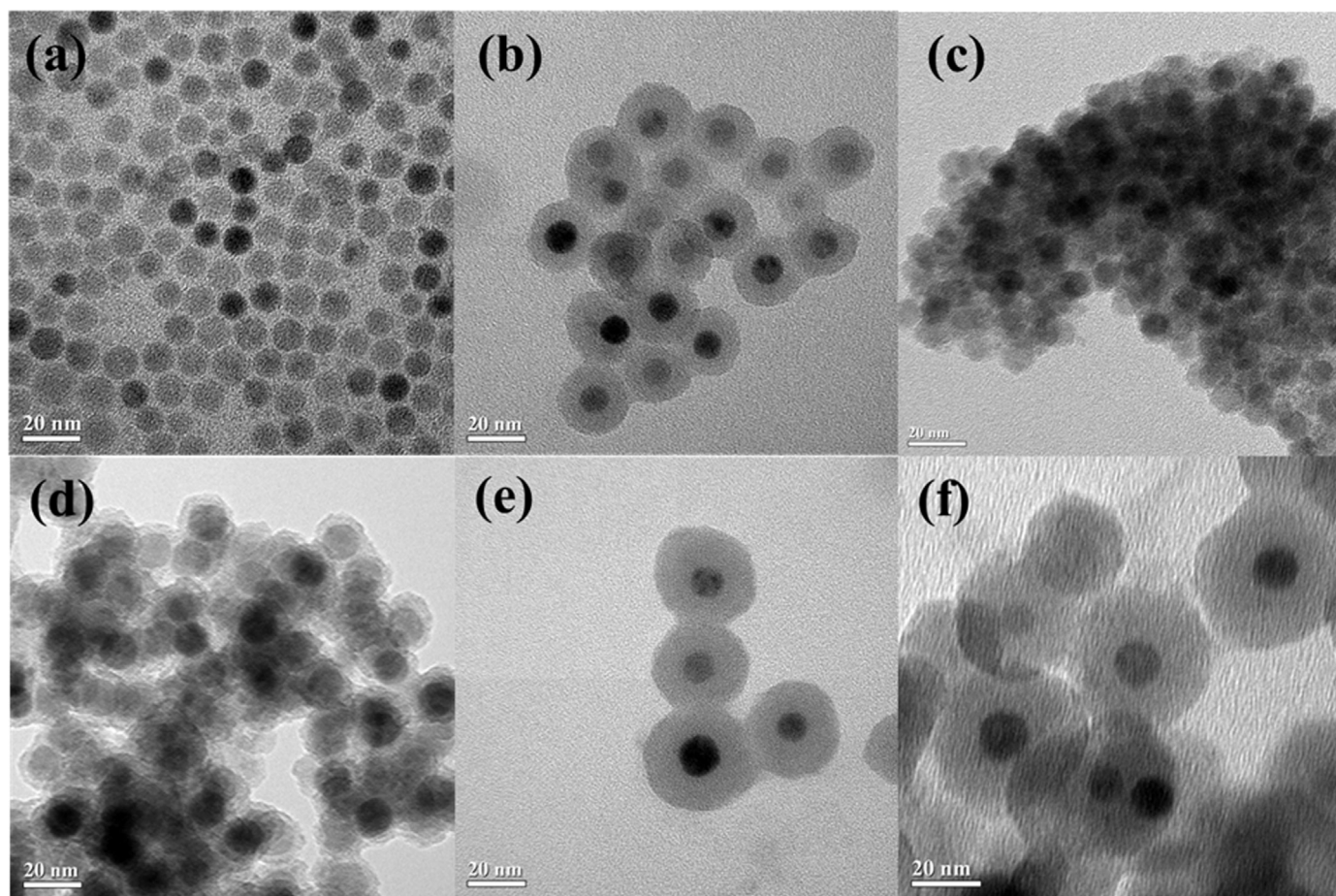


Fig. 2. The TEM images of (a) iron oxide nanoparticles, (b) silica-coated iron oxide, (c) titania-coated iron oxide (TI) nanocomposites, (d) TSI nanocomposites_Sample A (TEOS 150 μ L), (e) TSI nanocomposites_Sample B (TEOS 600 μ L), (f) TSI nanocomposites_Sample C (TEOS 2400 μ L).

Table 1

Differences in quantities of TEOS added in the syntheses and silica layer thicknesses measured using TEM for the titania-silica-iron oxide (TSI) nanocomposites.

TSI sample	TEOS added (μ L)	Silica shell thickness (nm) ^a	Sizes of TSI nanocomposites (nm) ^b	Polydispersity Index (PDI) of TSI samples ^b
A	150	1.1 \pm 0.5	98.2 \pm 28.09	0.2448
B	600	6.1 \pm 1.2	108.5 \pm 28.86	0.2113
C	2400	16.6 \pm 2.0	117.2 \pm 42.9	0.2252

^a Measured from the TEM images of the corresponding silica-coated iron oxides nanoparticles (SI) shown in Fig. S1 (Supplementary).

^b Measured from dynamic light scattering (DLS) analysis.

recombination center of photogenerated electron and hole as shown in Fig. 4. Therefore, less reactive oxygen species (such as hydroxyl radicals) were generated on the surface of TI nanocomposite under UV irradiation for degradation of methylene blue. Consequently, TI nanocomposites with the direct contact between iron oxide and titania exhibited low photocatalytic activity. Insertion of silica, a large bandgap insulating material, demonstrated significantly higher in photocatalytic activities likely due to the prevention of electron transfer between titania and iron oxide and decrease in the recombination of electron and hole.

Moreover, the results revealed that the degradation efficiency was found to depend essentially on the thickness of silica interlayer. In TSI_Sample A with thin silica layer, the photodegradation of methylene blue decreased by more than 10% comparing to the ones with thicker layer. The reasons for the higher photocatalytic activities when

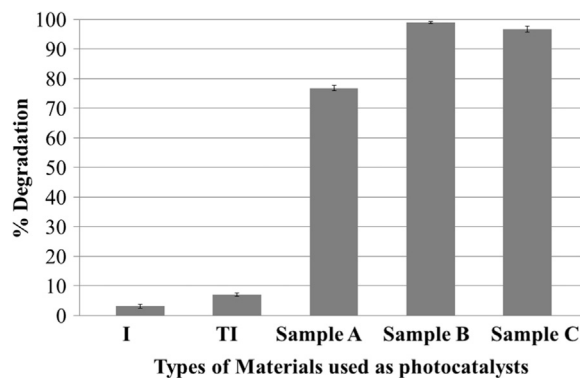


Fig. 3. Comparison of photocatalytic degradation of four samples: iron oxide nanoparticles (I), titania coated iron oxide nanoparticles (TI), titania-silica-iron oxide nanocomposites with 1 nm silica interlayer (TSI_sample A), titania-silica-iron oxide nanocomposites with 6 nm silica interlayer (TSI_sample B), titania-silica-iron oxide nanocomposites with 16.6 nm silica interlayer (TSI_sample C).

thicker silica interlayer was inserted could be due to the incomplete silica coating when thin silica layer was fabricated. Another explanation for the silica thickness dependence of photocatalytic activities could be because of quantum tunneling of electrons through the thinner silica layer similar to other three layer systems previously reported [26]. From our observation, the silica layer thickness of 6 nm was suitable for preventing the interaction between iron oxide nanoparticles and titania nanoparticles and encouraged the adsorption of dye molecules on surface of catalyst leading to high photocatalytic activities of the TSI nanocomposites.

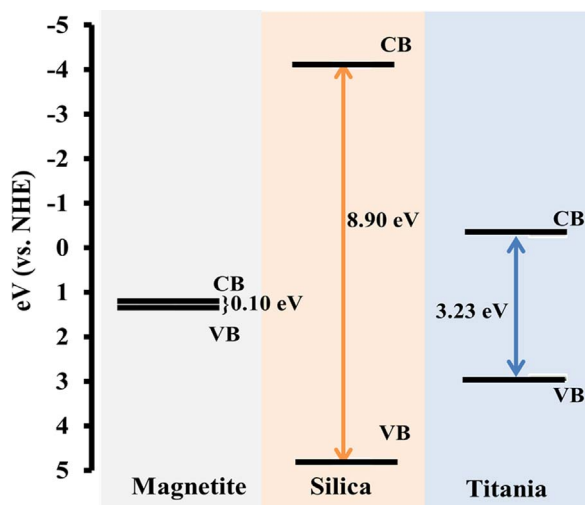


Fig. 4. Band edge positions of the three materials in composites [23–25].

To test the reusability of TSI nanocomposites on the photocatalytic methylene blue degradation, the photocatalysts could maintain high photocatalytic activity and could be easily recovered by a magnet (Fig. 5). The photocatalyst was reused at least three times without regeneration. After three cycles, degradation of methylene blue decrease to lower than 90%, likely due to the incomplete photodegradation in previous steps that could lead to by-products deposition onto the active surface of TSI. The regeneration of the photocatalyst could be done by addition of 35 wt% hydrogen peroxide solution as suggested previously [27].

Other than photodegradation of organic dyes, the titania-based photocatalysts have been reported to exhibit bactericidal activity [14]. Therefore, the modified titania nanocomposite, TSI_Sample B, was tested for its bactericidal activity against *S. aureus*. After treating exponential phase cells of *S. aureus* with TSI under long wavelength UV light, the number of survival cells was dramatically decreased to 0.5×10^5 CFU/mL, comparing to the untreated control (2.5×10^6 CFU/mL) (Fig. 6). In contrast, treating *S. aureus* with UV light alone caused no effect on bacterial survival relative to the untreated control (Fig. 6). It obviously revealed that the TSI nanocomposite activated with UV

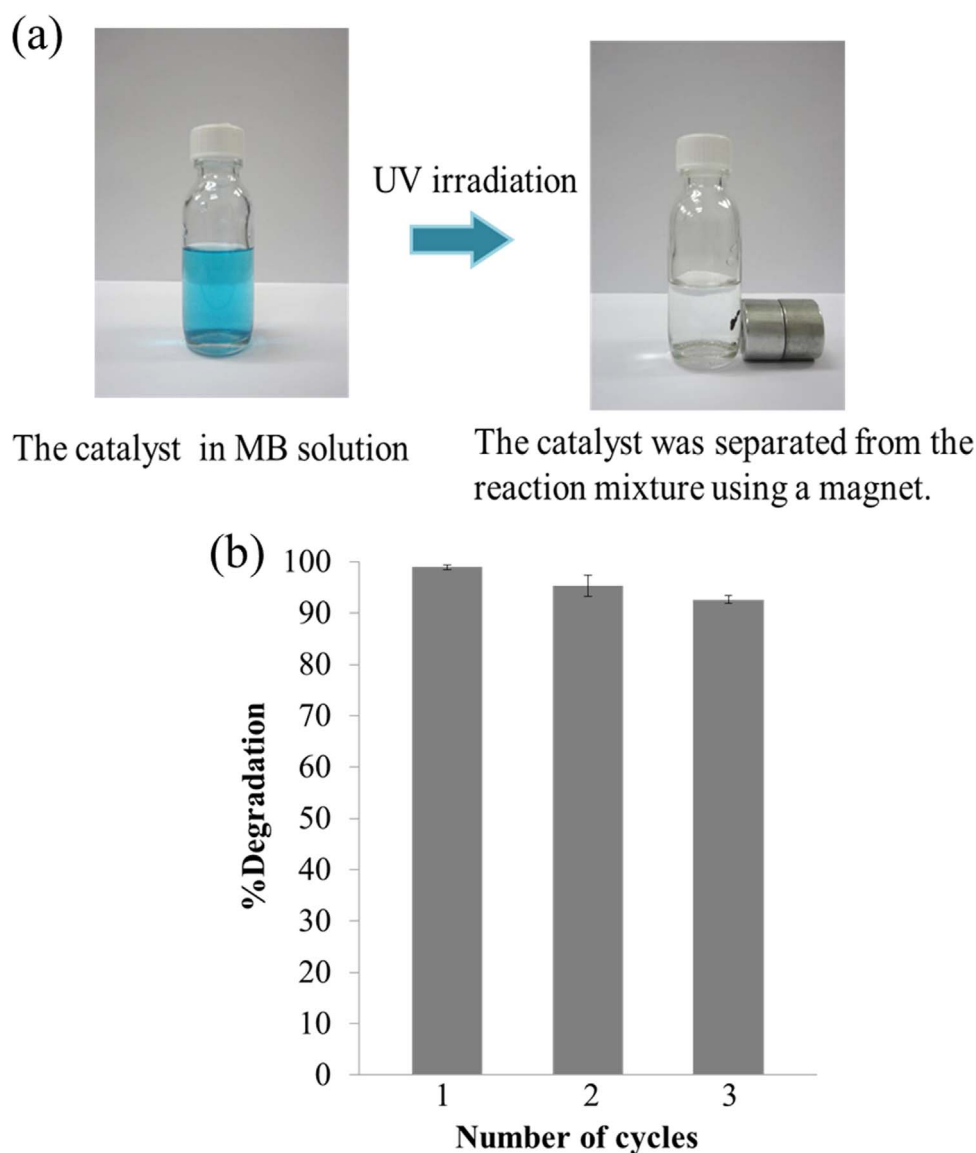


Fig. 5. (a) Illustration of a magnetic separation of titania-silica-iron oxide nanocomposites from methylene blue solution (b) Photocatalytic degradation of methylene blue by recycled TSI nanocomposites.

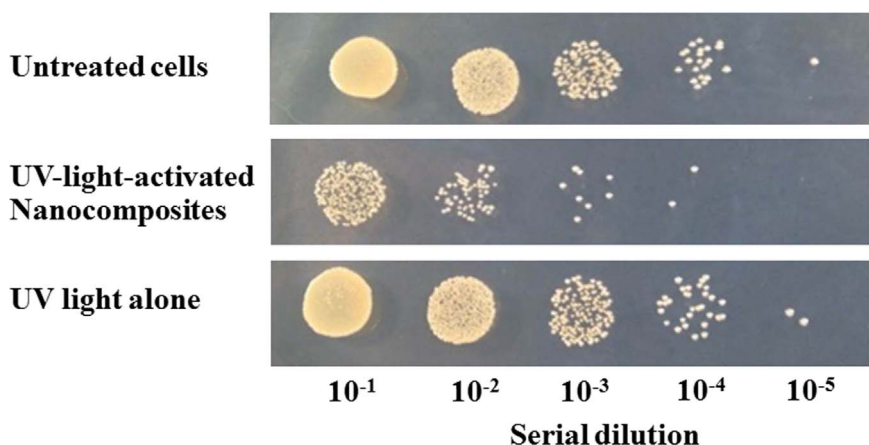


Fig. 6. The bactericidal activity of TSI_Sample B in *S. aureus* treated with UV-light-activated nanocomposites (Panel 2) and UV light alone (Panel 3), comparing to untreated cells (Panel 1).

light could effectively kill *S. aureus*. The cytotoxicity of TSI nanocomposite against *S. aureus* is probably due to a photocatalytic oxidation of nanocomposite, which generates reactive radicals, leading to depolarization of bacterial outer membrane [28,29]. In addition, the light that is required for activating photocatalytic activity of TSI is a long wavelength which is harmless to biological molecules. Thus, it is safe to use TSI for further applications. Usually, only short wavelength of UV is known as a mutagen causing DNA damages in both prokaryotic [30] and eukaryotic cells [31]. Altogether, the results suggest that TSI nanocomposites exhibited bactericidal activity against *S. aureus*, indicating that it could be used as an alternative treatment for bacterial infections as well as for cleaning the medical devices or hospital textiles which are the most common sources for HAI [32]. Due to TSI has magnetic properties, it can be easily separated from contaminated sources and simply reusable. However, the application of TSI as disinfectant needs further optimization and is worth to investigate.

4. Conclusions

Magnetic photocatalysts (titania-silica-iron oxide nanocomposites) with high photocatalytic properties and magnetic response have been successfully synthesized. These composites showed higher efficiency for the decomposition of methylene blue compared with titania-coated iron oxide nanoparticles and iron oxide nanoparticles. The composites were reused at least three times without any regeneration. The thickness of silica interlayer of at least 6 nm was enough to obtain the nanocomposites with high photocatalytic activities. With this high photocatalytic activities and its reusability, TSI can possibly be used in environmental approach such as a photodegradation of organic pollutants in polluted area.

Moreover, titania-silica-iron oxide nanocomposites also showed the bactericidal effects on pathogenic microorganism model *S. aureus*. Therefore, this antibacterial activity of TSI could be applied in medical applications, including alternative treatments for bacterial infection and novel agent for disinfecting contaminated sources in hospital settings.

Acknowledgment

This work was financially supported by the Thailand Research Fund (MRG5680091) and partly by the Grants for Development of New Faculty Staff, Ratchadaphiseksomphot Endowment Fund, Chulalongkorn University. We would like to thanks Dr. Paiboon Vattanaviboon for critical discussion. We are also grateful to Dr. Kritapas Laohhasurayotin for providing assistance in VSM measurement and Mr. Boonlaer Ngotawornchai for his assistance with the TEM imaging.

Appendix A. Supplementary material

Supplementary data associated with this article can be found in the online version at [doi:10.1016/j.jmmm.2016.10.123](https://doi.org/10.1016/j.jmmm.2016.10.123).

References

- [1] K. Pirkanniemi, M. Sillanpää, Chemosphere 48 (2002) 1047–1060.
- [2] A. Fujishima, T.N. Rao, D.A. Tryk, J. Photochem. Photobiol. C 1 (2000) 1–21.
- [3] X. Chen, S.S. Mao, Chem. Rev. 107 (2007) 2891–2959.
- [4] D. Beydoun, R. Amal, G. Low, S. McEvoy, J. Phys. Chem. B 104 (2000) 4387–4396.
- [5] D. Beydoun, R. Amal, G. Low, S. McEvoy, J. Mol. Catal. A: Chem. 180 (2002) 193–200.
- [6] X. Yu, S. Liu, J. Yu, Appl. Catal. B 104 (2011) 12–20.
- [7] Z. Teng, X. Su, G. Chen, C. Tian, H. Li, L. Ai, G. Lu, Colloids Surf. A 402 (2012) 60–65.
- [8] J. Park, K. An, W. Hwang, J.G. Park, H.J. Noh, J.Y. Kim, J. Park, N. Hwang, T. Hyeon, Nat. Mater. 3 (2004) 891–895.
- [9] X. Wen, J. Yang, B. He, Z. Gu, Curr. Appl. Phys. 8 (2008) 535–541.
- [10] C. Meiorin, D. Muraca, K.R. Pirota, M.I. Aranguren, M.A. Mosiewicki, Eur. Polym. J. 53 (2014) 90–99.
- [11] L. Shen, Y. Qiao, Y. Guo, S. Meng, G. Yang, M. Wu, J. Zhao, Ceram. Int. 40 (2014) 1519–1524.
- [12] M. Tadic, S. Kralj, M. Jagodic, D. Hanzel, D. Makovec, Appl. Surf. Sci. 322 (2014) 255–264.
- [13] M. Abbas, M.N. Islam, B.P. Rao, M.O. Abdel-Hamed, C. Kim, J. Ind. Eng. Chem. 31 (2015) 43–46.
- [14] J. Wang, J. Li, S. Qian, G. Guo, Q. Wang, J. Tang, H. Shen, X. Liu, X. Zhang, P.K. Chu, ACS Appl. Mater. Interfaces 8 (2016) 11162–11178.
- [15] C.J. Chen, Y.C. Huang, Clin. Microbiol. Infect. 20 (2014) 605–623.
- [16] A.C. Fluit, J. Acar, M.E. Jones, R. Gupta, F.J. Schmitz, J. Verhoef, Clin. Infect. Dis. 30 (2000) 454–460.
- [17] M.L. Metersky, R.G. Masterton, H. Lode, T.M. File Jr., T. Babinchak, Int. J. Infect. Dis. 16 (2012) e321–e331.
- [18] V.G. Fowler, J.M. Miro, B. Hoen, C.H. Cabell, E. Abrutyn, E. Rubinstein, G.R. Corey, D. Spelman, S.F. Bradley, B. Barsic, P.A. Pappas, K.J. Anstrom, D. Wray, C.Q. Fortes, I. Anguera, E. Athan, P. Jones, J.T.M. van der Meer, T.S.J. Elliott, D.P. Levine, A.S. Bayer, JAMA 293 (2005) 3012–3021.
- [19] D.K. Yi, S.S. Lee, G.C. Papaefthymiou, J.Y. Ying, Chem. Mater. 18 (2006) 614–619.
- [20] H.L. Ding, Y.X. Zhang, S. Wang, J.M. Xu, S.C. Xu, G.H. Li, Chem. Mater. 24 (2012) 4572–4580.
- [21] Z. Liu, Z. Jian, J. Fang, X. Xu, X. Zhu, S. Wu, Int. J. Photoenergy 2012 (2012), 702503.
- [22] B. Prapagdee, P. Vattanaviboon, S. Mongkolsuk, FEMS Microbiol. Lett. 232 (2004) 217–223.
- [23] Y. Wang, R. Zhang, J. Li, L. Li, S. Lin, Nanoscale Res. Lett. 9 (2014) 1–8.
- [24] X. Hou, Y. Tian, X. Zhang, S. Dou, L. Pan, W. Wang, Y. Li, J. Zhao, J. Alloy. Compd. 638 (2015) 214–220.
- [25] X. Lin, X. Guo, D. Liu, Q. Wang, H. Zhai, L. Chang, Mater. Res. Bull. 63 (2015) 72–79.
- [26] C.H. Liu, Y.C. Chang, T.B. Norris, Z. Zhong, Nat. Nanotechnol. 9 (2014) 273–278.
- [27] F. Nogueira, J. Lopes, A. Silva, M. Goncalves, A. Anastacio, K. Sapag, L. Oliveira, Appl. Clay Sci. 43 (2009) 190–195.
- [28] C. Fonseca, A. Ochoa, M.T. Ulloa, E. Alvarez, D. Canales, P.A. Zapata, Mater. Sci. Eng. C: Mater. Biol. Appl. 57 (2015) 314–320.
- [29] J. Liu, Z. Wang, Z. Luo, S. Bashir, Dalton Trans. 42 (2013) 2158–2166.
- [30] G. Villani, S. Boiteux, M. Radman, Proc. Natl. Acad. Sci. USA 75 (1978) 3037–3041.
- [31] S.T. Durant, K.S. Paffett, M. Shrivastav, G.S. Timmins, W.F. Morgan, J.A. Nickoloff, Mol. Cell. Biol. 26 (2006) 6047–6055.
- [32] S. Fijan, S.S. Turk, Int. J. Environ. Res. Public Health 9 (2012) 3330–3343.